


Tectonic inheritance and kinematic strain localization as trigger for the formation of the Helvetic nappes, Switzerland

Arthur Bauville^{1,2}  · Stefan M. Schmalholz³

Received: 30 May 2016 / Accepted: 13 January 2017 / Published online: 2 March 2017
© Swiss Geological Society 2017

Abstract The Helvetic nappes in Switzerland consist of sediments, which have been sheared off and thrust over the crystalline basement of the European passive continental margin during Alpine orogeny. Their basal shear zones usually root above the external crystalline massifs. However, the mechanisms that initiated the shear zones and the associated nappe formation are still debated. We perform two-dimensional numerical simulations of the shearing of linear viscous fluids above a linear viscous fluid with considerably higher viscosity (quasi-undeformable). The boundary between the fluid, mimicking the sediments, and the quasi-undeformable fluid, mimicking the basement, exhibits geometrical perturbations, mimicking half-grabens. These geometrical perturbations can trigger significant strain localization and the formation of shear zones within the linear viscous fluid although no rheological softening mechanism is active. This kinematic, ductile strain localization is caused by the half-grabens and the viscosity ratio between basement and sediments. The viscosity ratio has a strong control on the kinematics of strain localization, whereas the depth of the half-grabens has a weak control. For sediment viscosities in the order of 10^{21} Pas and typical half-graben geometries of 5 km

depth and 25 km width the localization generates (a) low-angle shear zones at the basement-sediment interface, but also entirely within the sediments, (b) horizontal transport >10 km associated with the shear zones, (c) shear zones with thickness in the order of 100 m, (d) an ordered stacking of model nappes and (e) shear zones that root above the basement. The results suggest that tectonic inheritance in the form of half-grabens and associated kinematic strain localization could have been the triggering mechanism for Helvetic nappe formation, and not rheological softening mechanisms, which might, however, have subsequently further intensified shear localization significantly.

Keywords Tectonic inheritance · Kinematic strain localization · Helvetic nappes · Wedge

1 Introduction

During Alpine orogeny, parts of the sedimentary cover of the European passive margin have been sheared off and thrust over the crystalline basement whereby the pre-Alpine basement topography was characterized by half-grabens and horsts (e.g. Trümpy 1960). The half-grabens and horsts represent a tectonic inheritance from an earlier rifting event. At present the sheared and displaced sedimentary units form sedimentary nappes within the Helvetic nappe system of Switzerland (Fig. 1). Parts of the crystalline basement, including autochthonous cover sediments, have also been deformed and form the external crystalline massifs (e.g. Ménot et al. 1994). The sedimentary nappes have been displaced over more than 10 km along low angle shear zones. However, the mechanisms responsible for triggering and forming these shear zones are still incompletely understood.

Editorial handling: C. Sue and S. Schmid.

✉ Arthur Bauville
abauville@jamstec.go.jp

¹ Department of Mathematical Science and Advanced Technology (MAT), Japan Agency for Marine-Earth Sciences and Technology (JAMSTEC), Yokohama, Japan

² Geophysics and Geodynamics Group, Institute of Geosciences, Johannes Gutenberg University, Mainz, Germany

³ Institute of Earth Sciences, University of Lausanne, Lausanne, Switzerland

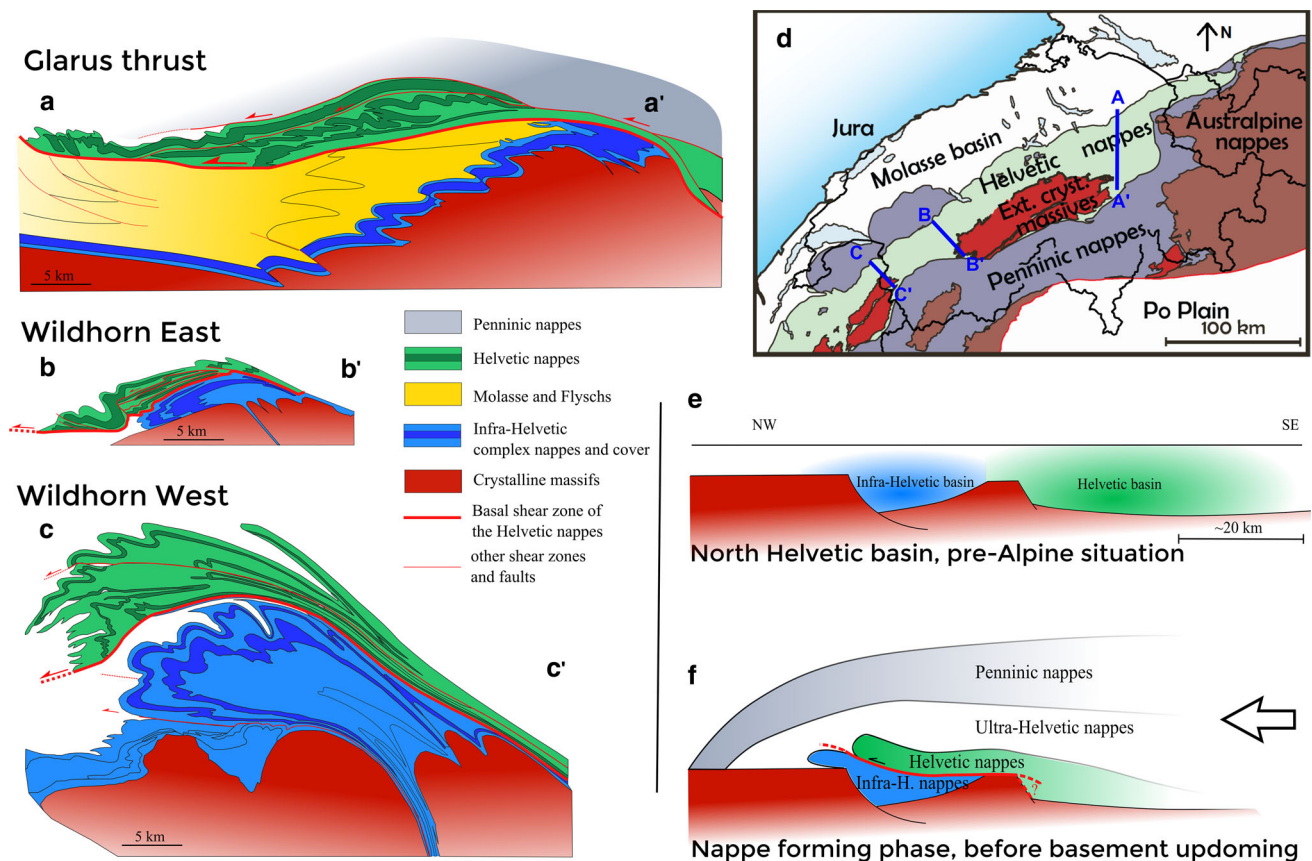


Fig. 1 Simplified geological cross sections across the Helvetic nappe system (a–c) and conceptual model of its evolution (e, f). The simplified tectonic map in d shows the location of the cross sections. a–c Cross sections across the Helvetic nappe system in Eastern, central and western Switzerland, respectively (after Pfiffner 1993; Herwegh and Pfiffner 2005; Escher et al. 1993, respectively). The Helvetic nappes are thrust along a prominent basal shear zone (thick red line) over the Infra-Helvetic complex (b, c) and over

Geologic reconstructions suggest that the sediments in structurally higher nappes have been deposited in more distal (SE direction) regions of the passive margin (Fig. 1; e.g. Masson et al. 1980). The sedimentary units forming individual nappes have been attributed to different depositional domains related to the paleo-topography of the pre-Alpine European basement (Fig. 1). The lowermost nappes in Western Switzerland are fold nappes (Morcles and Doldenhorn nappes; parts of the so-called Infrahelvetic complex; Epard 1990; Pfiffner 1993) and consist of sediments that have been deposited in the North-Helvetic basin which is interpreted as a half-graben (Epard 1990). The uppermost nappes are more similar to thrust sheets (so-called Helvetic nappes, e.g. Wildhorn nappe) and have been deposited in the more distal Helvetic domain (basin) which was separated from the North-Helvetic basin by a horst (e.g. Epard 1990). In Eastern Switzerland, the Glarus thrust sheet has been sheared over more proximal basement, autochthonous Mesozoic sediments and Flysch units whereby the Infrahelvetic units did not form

Molasse and Flysch sediments (a). The cross sections are parallel to the displacement direction of the nappes. e Conceptual palinspastic reconstruction of the European margin in Western and Central Switzerland. f Conceptual model of nappe emplacement: sediments initially filling distal basins are displaced tens of kilometers over more proximal basement and sediment units while acquiring their typical nappe geometry (modified after Steck 1984; Bugnon 1986)

a fold nappe as in Western Switzerland (Fig. 1; Siegenthaler, 1974). The basal shear zones of the tectonic nappes are often (a) continuous over more than 10 km, (b) subhorizontal, and (c) root in the external crystalline massifs (Fig. 1, see also Pfiffner et al. 2011).

Many studies argue that softening mechanisms are required to generate ductile shear zones and that basal shear zones during nappe displacement are weaker than the less deformed rocks forming the nappe (e.g. Poirier 1980; Austin et al. 2008). Therefore, different thermo-mechanical processes have been suggested for the softening of basal shear zones, such as grain size reduction in combination with grain size sensitive diffusion creep (e.g. Ebert et al. 2008; Austin et al. 2008), higher temperatures at the base of the nappe in combination with a temperature-dependent viscosity (e.g. Bauville et al. 2013) or combined shear heating and fluid release by carbonate decomposition (e.g. Poulet et al. 2014). In contrast, we show in this study that basal shear zones can also be initiated and maintained

during finite strain deformation in a linear viscous fluid without any softening mechanism.

Structural observations, such as the buttressing of sediments against the crystalline massif in the Ecrins and Bourg d'Oisan massifs in France (Gillcrist et al. 1987, Dumont et al. 2008, Bellanger et al. 2014), indicate that the basement was more competent (i.e. having a higher mechanical strength or greater resistance to deformation) than the sedimentary cover. The increase of strain towards the base of spreading-gliding nappes is another example for such competence contrast (e.g. Brun and Merle 1985; Merle 1986). The impact of the basement-cover competence contrast on nappe formation has been studied with analogue experiments and numerical simulations. For example, experiments showed that the indentation of a viscous material by a rigid object leads to the formation of a shear zone above the rigid indenter and the subsequent formation of a viscous fold nappe (e.g. Bucher 1956; Merle and Guillier 1989). Similar results have been obtained with numerical simulations (Duretz et al. 2011). Also, Wissing and Pfiffner (2003) showed with viscoplastic numerical simulations that the formation of a nappe with a prominent basal shear zone can be triggered by a rigid obstacle which mimicked a basement high. In their model the shear zone extends horizontally past this rigid obstacle. They applied a configuration with a weaker decollement unit which is entrained at the base of the nappe to enhance and maintain the basal shear zone. Furthermore, Bauville and Schmalholz (2015) performed thermo-mechanical numerical simulations for basement-cover deformation considering a viscoelastoplastic rheology with a nonlinear (power-law) and temperature dependent viscosity (Fig. 2). They performed a systematic analysis of the simulations and determined the conditions for which the basement-cover deformation is dominated by a thin-skinned or thick-skinned style of deformation. In their simulations horizontal shear zones also formed at the basement-cover interface. The formation of ductile shear zones at the interface of the more competent basement with the less competent sediments is not surprising since it is known in fluid dynamics that shear zones can form in a linear viscous, non-localizing fluid around a rigid obstacle. These shear zones are known as boundary layers and are responsible, for example, for skin friction on airplanes (e.g. Prandtl 1904; Schlichting and Gersten 2017). Different to such boundary layer shear zones, the thermo-mechanical simulations of Bauville and Schmalholz (2015) also show the formation of shear zones entirely within the sediments of the half grabens (Fig. 2). Some of their results further suggest that such shear zones can also form if the sediments are described by a linear viscous fluid. In this study, we extend and elaborate the simulations with linear viscous fluids performed by Bauville and Schmalholz (2015) in order to quantify shear localization in a non-localizing, linear viscous fluid

(mimicking sediments) which is sheared over a rigid material with laterally-varying topography (mimicking basement with half grabens). Following earlier nomenclature, we refer to such a strain localization process in a linear viscous fluid as kinematic strain localization (e.g. Brun, 2002; Braun et al. 2010). Kinematic strain localization can be caused by the applied boundary conditions (e.g. a velocity discontinuity; Brun 2002), the geometrical configuration (e.g. flow around a rigid obstacle or particular shear zone geometry; Braun et al. 2010) or internal variations in mechanical strength, such as the viscosity variation (due to thermal gradient) in channel flow models (e.g. Bauville and Schmalholz 2015).

The aims of this study are (a) to show that significant shear localization can occur within a linear viscous fluid if it is sheared above a rigid material with topography mimicking half-grabens, (b) to quantify the shear localization and shear zone thickness inside the linear viscous fluid, (c) to study the impact of half-graben depth and fluid viscosity on shear localization and (d) to argue that the pre-Alpine basement topography, which represents the tectonic inheritance from earlier rifting, could have triggered shear zone formation within sediments and hence played an important role in the initiation of thrusting of the Helvetic nappes over the Infrahelvetic complex.

2 Method and model

2.1 Numerical method

The applied 2-D numerical algorithm solves the Stokes equations including gravity, which describe the flow of an incompressible fluid where inertial forces are negligible compared to viscous forces. Equations account for the conservation of momentum and mass (e.g. Mase 1970). The numerical model is based on the Galerkin finite element method and uses the software MILAMIN (Dabrowski et al. 2008) to solve the governing system of equations. The algorithm further uses the mesh-generator Triangle (Shewchuk 2002) to generate a Lagrangian unstructured mesh composed of seven-node Crouzeix-Raviart triangular elements with three discontinuous pressure nodes. Material boundaries are defined by contour lines that are used to generate a new mesh when the finite elements become too distorted. The governing equations and the numerical algorithm are described in detail in Schmalholz et al. (2014).

2.2 Model geometry and material properties

The model configuration mimics an idealized and simplified upper crustal region of a passive margin, where the basement includes half grabens and is overlain by sediments (Fig. 1e, 2). Fold nappes and thrust sheets in the

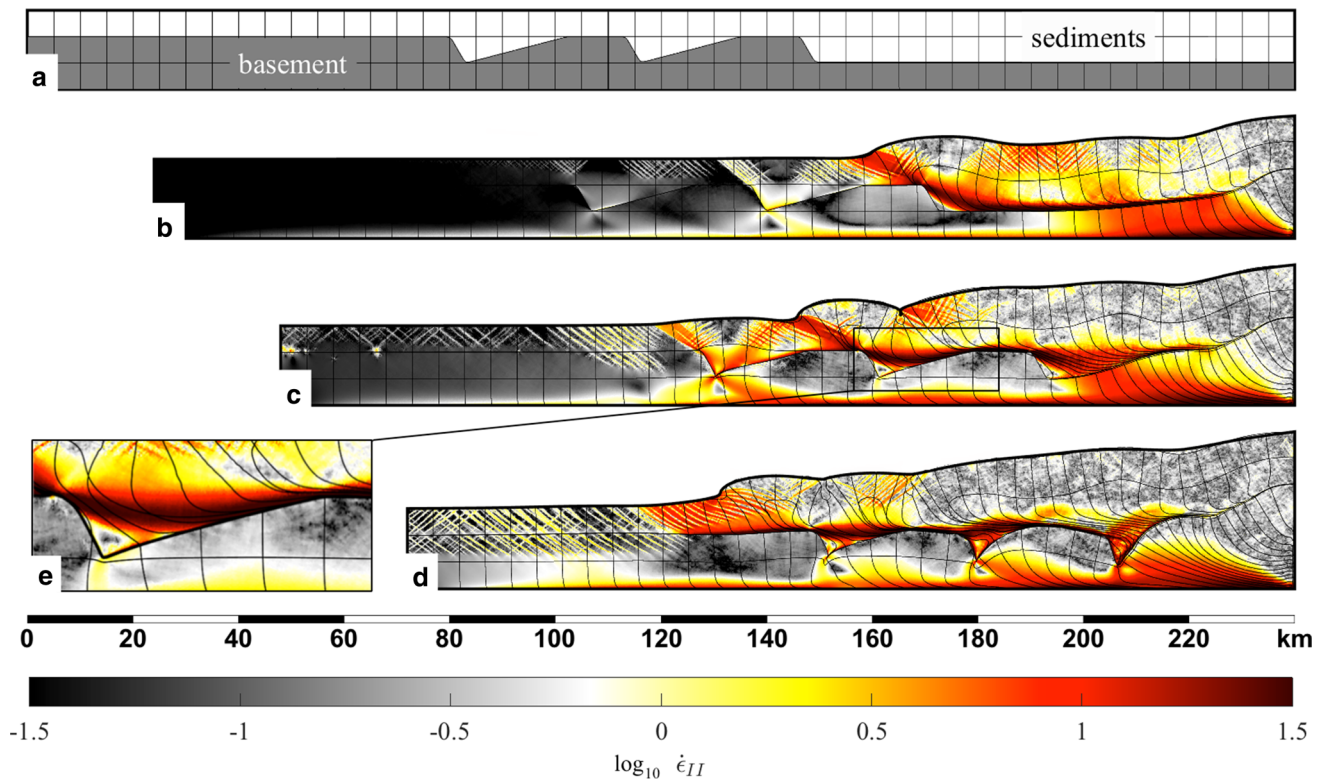


Fig. 2 Evolution of a representative simulation (TM-e) from Bauville and Schmalholz 2015. The geometry mimics an idealized passive margin geometry with basement half-grabens. Boundary conditions are the same as in this study. Rheology of the basement and sediment is viscoelastoplastic with a power-law ($n = 4$)

Helvetic nappe system typically formed at 8–15 km depth (e.g. Kirschner et al. 1995). To avoid modeling the burial stage of the passive margin evolution, sediments are already 5 km thick in the initial configuration. The half grabens are maximal 5 km deep and 25 km long, in agreement with reconstructions for the North Helvetic basin in Western Switzerland (Boutoux et al. 2014, and Jean-Luc Epard, personal communication). The model consists of three linear viscous fluids representing from bottom to top the basement and two sedimentary layers with viscosities of 10^{23} , 10^{21} and 10^{22} Pa s, respectively. A basement viscosity of 10^{23} Pa s generates a deviatoric stress in the order of 100 MPa for a tectonic shortening rate of 10^{-15} s^{-1} , which is a stress in agreement with the predictions of Byerlee's law at depths between 6 to 10 km, and, which is supported by borehole stress measurements (Townend and Zoback 2000). The top, stronger sediment layer represents the stronger upper part of sediments around the brittle-ductile transition (e.g. overlying Penninic nappes), while the lower, weaker layer represents the more ductile sediments eventually forming the Helvetic nappes (Fig. 3). The density of the material is 2500 kg m^{-3} . The impact of temperature and erosion is neglected in the simple models.

temperature dependent viscosity. During compression sediments are sheared over the deforming basement. Shear zones form in the sediment. The shear zones are initiated at the basement-cover interface and cut horizontally through the half grabens

The applied velocity boundary conditions mimic model configurations of typical analogue sandbox experiments which have been applied to study the formation of accretionary wedges (see Buiter 2012; Graveleau et al. 2012 for recent reviews). A horizontal velocity is applied to the left and bottom boundaries (Fig. 3). This velocity is updated every time step to maintain a constant bulk shortening rate of 10^{-15} s^{-1} . The right wall is fixed in the horizontal direction, thus acting as a backstop. Vertical velocity is zero at the bottom boundary, while left and right boundaries are free to slip (Fig. 3). The top boundary is a free surface.

2.3 Strain and displacement quantification

For every numerical time step, having index i , and at each point of a finely resolved passive grid we compute the incremental deformation tensor, G^i ,

$$G^i = \begin{bmatrix} 1 + \Delta t \frac{dv_x^i}{dx} & \Delta t \frac{dv_x^i}{dy} \\ \Delta t \frac{dv_y^i}{dx} & 1 + \Delta t \frac{dv_y^i}{dy} \end{bmatrix} \quad (1)$$

where Δt , v_x^i , v_y^i , x and y are the time step, the velocity in the horizontal x -direction at time step i , the velocity in the

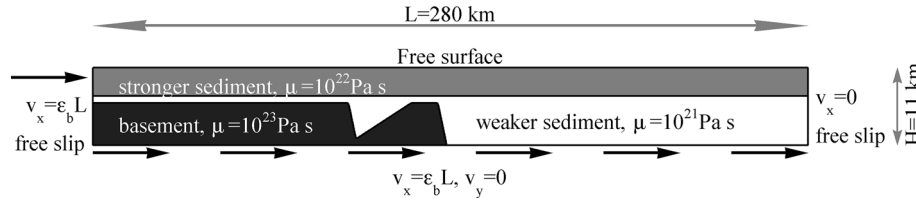


Fig. 3 Initial configuration of the model. The geometry represents a simplified passive margin. μ is the viscosity of the material; v_x and v_y are horizontal and vertical velocities respectively; $\varepsilon_b = 10^{-15} \text{ s}^{-1}$ is the bulk shortening rate

vertical y -direction at time step i , the horizontal x -coordinate and the vertical y -coordinate, respectively (e.g. Frehner and Schmalholz 2006). For a given point the finite deformation tensor F is computed by multiplying all the incremental deformation tensors for all time steps, that is, $F = \prod_{i=1}^{ni} G^i$ where ni is the total number of time steps. The maximum and minimum principal stretch axes, e_1 and e_2 , respectively, correspond to the square root of the maximum and minimum eigenvalues, respectively, of the tensor $F^T F$ (superscript T represents the transpose of the tensor) which is the right Cauchy-Green strain tensor (Bower 2009). We quantify strain with the maximum shear strain γ_m which is (Ragan 2009; Beer and Erj 2014)

$$\gamma_m = e_1 - e_2 \quad (2)$$

The maximum relative displacement, D_r , in the direction of maximum shear along any profile perpendicular to the direction of maximal shear strain is computed according to:

$$D_r(h) = \int_0^h \gamma_m dh, \quad (3)$$

where h is the distance along the profile. We calculated the integral numerically from the numerical results. The displacement D_r is used to quantify the relative displacement across a shear zone. This displacement quantification assumes that the shear zone is dominated by simple shear which is the case in the simulations.

To describe horizontal displacement at the scale of the entire model we also compute the horizontal displacement, D_h , of individual points in the model with

$$D_h = X_{pg}^{ini} - X_{pg}, \quad (4)$$

where X_{pg}^{ini} and X_{pg} are the initial and final horizontal coordinates of a particular point in the model, respectively.

3 Results

With increasing bulk shortening, the initially flat model having a constant thickness forms a viscous wedge with the largest thickness at the backstop (on the right boundary of the model; Fig. 4) and the smallest thickness to the left and moving boundary of the model. During shortening, the

sediments in the rightmost wide basin (green) are compressed, extruded from their basin and sheared over the basement (black) to the left (Fig. 4). The (green) sediments are sheared also over the sediments (dark blue) which fill the half-graben to the left. The interface between the dark and light green regions is folded and deformed into a fold nappe with an overturned limb, a frontal part and a normal limb (Fig. 4g). The normal and the inverted limb are sub-horizontal after 50% bulk shortening. In the final stage of shortening (Fig. 4e, f) the higher parts of the dark blue sediments have been sheared out of their half-graben while the lower sediments remain inside the half-graben (Figs. 4f, 3g). After 50% shortening the initial horizontal succession of sedimentary domains (colored domains) has been transformed into a vertical stack of nappes. The most internal (right) domains are found at the highest structural levels of the stack, that is, white sediments are at the bottom, blue ones in the middle and green ones are highest (Fig. 4f, g).

The quantities to describe the deformation in the model after 50% bulk shortening are shown in Fig. 4. The region shown in Figs. 4a–d corresponds to the one shown in Fig. 3g. The black framed region in Fig. 4a–d is shown enlarged in Fig. 4e, f. Since the model materials are linear viscous, the viscosity of each model unit is constant (Fig. 5a). The strain rate distribution (Fig. 5b) shows that strain rates in the sediments are ~ 10 times higher than the average background strain rate (i.e. $\sim 10^{-14} \text{ s}^{-1}$) in the sedimentary nappe pile. Strain rates decrease below 10^{-15} s^{-1} in the lowest part of the half-graben but reach a maximum of $\sim 10^{-13.5} \text{ s}^{-1}$ directly above the horizontal basement-sediment interface on the left of the half-graben. Overall, the strain rate distribution is smooth and does not show any significant localization within a region of constant viscosity, only at the interface between two model units of different viscosity, e.g. basement-sediment interface (Fig. 5b). In contrast, the horizontal displacement (Figs. 4e, 5c) shows a sharp variation at the interface between the green and blue sediments (see Fig. 4g for nappe geometry). We refer to the interface between the blue and green sediments in the following as a nappe boundary. Along a 1 km long profile across this nappe boundary the horizontal displacement varies from ~ 10 km

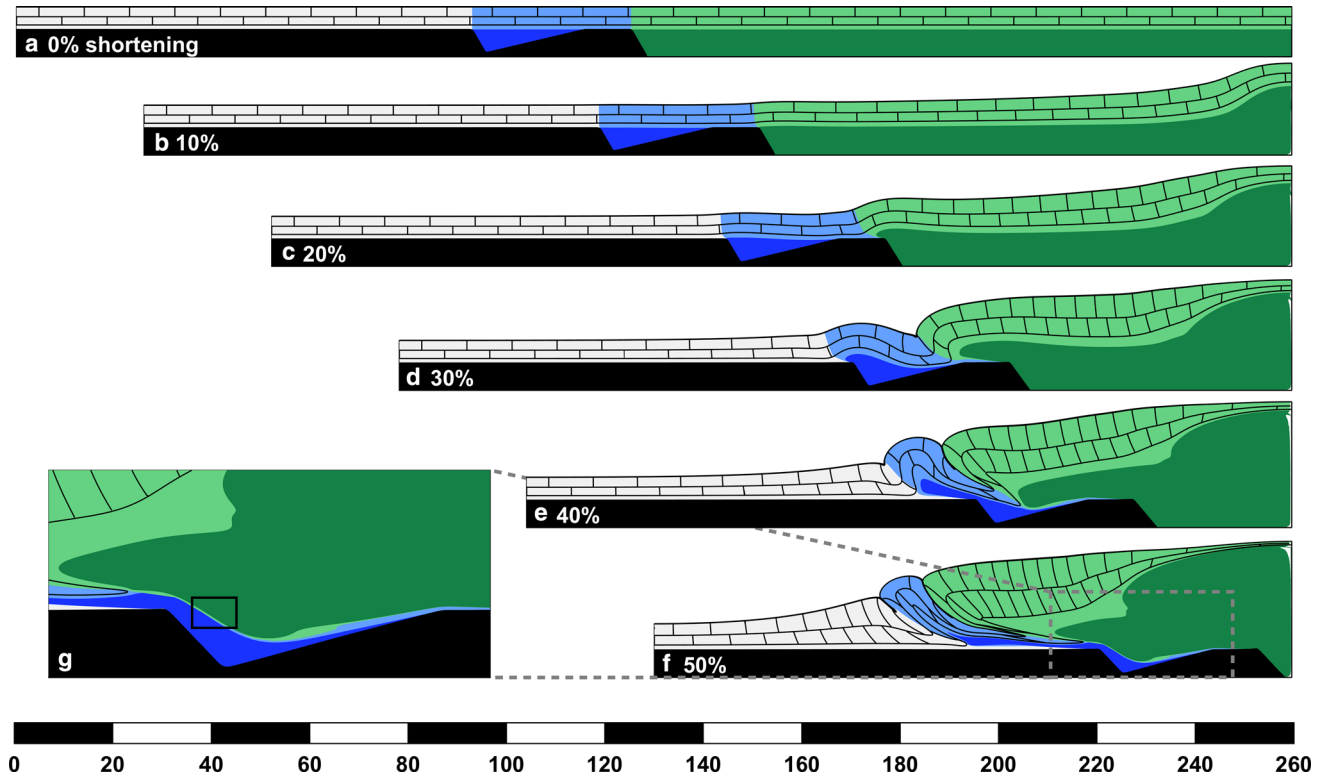


Fig. 4 a–f Evolution of the geometry of the model with increasing shortening. Basement is in black and sediments are colored. Limestone pattern indicates the stronger sediment, while the weaker

sediments bear no patterns. Colored areas are used as passive markers of the deformation. **g** Detail of the nappe structure at 50% shortening. The black frame indicates the area of focus for Fig. 4e, f

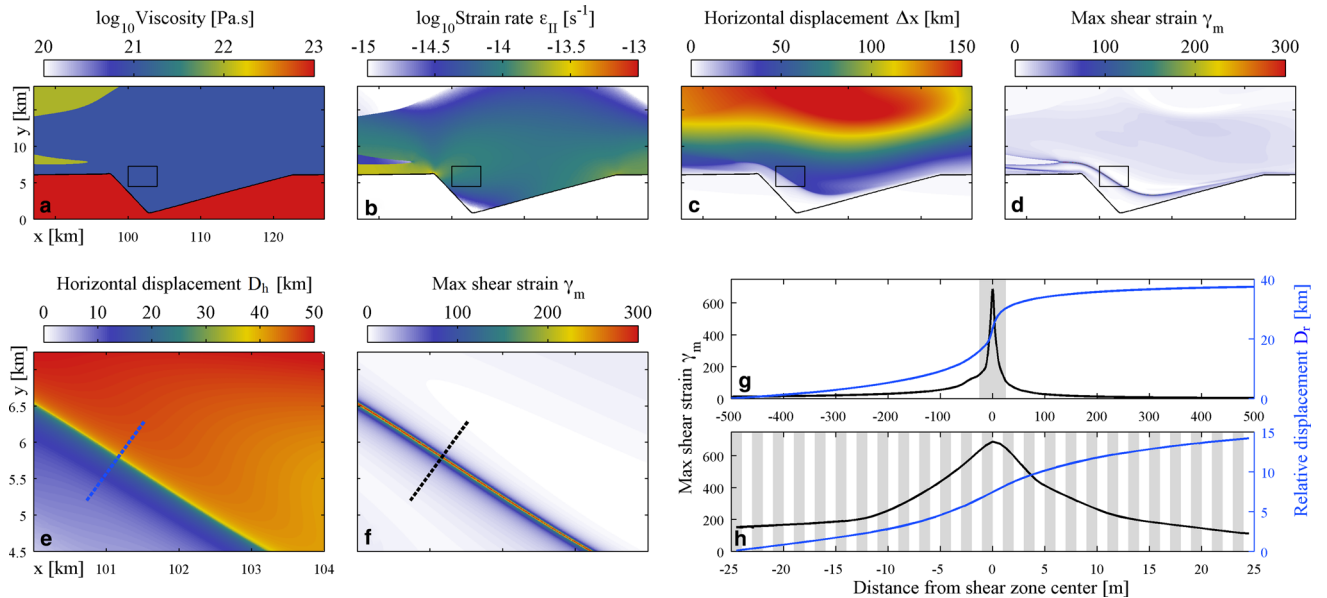


Fig. 5 Dynamic quantities describing the state of material properties and deformation at 50% shortening. Nappe geometry of the area featured in (a–d) is shown in Fig. 3g. Area of (e, f) is indicated by the

black frame in (a, d). **g** Maximum shear strain and relative displacement along the profile featured in (e, f). **h** Detail of the profile, indicated as the grey area in (g)

below to 50 km above the nappe boundary (blue dashed line in Fig. 4e). The relative displacement along this 1 km long profile is shown in Fig. 4g, h. The considerable

displacement variation across the nappe boundary is also expressed by a peak in the maximum shear strain (Fig. 4d, f–h). The maximum shear strain γ_m amounts to ~ 750 (i.e.

750 m of displacement across a 1 m thick shear zone; Fig. 5h). The width of the shear zone in which $\gamma_m > 375$ (i.e. half the maximal value in the shear zone) is ~ 10 m (Fig. 5h). The relative displacement, D_r , along the 1 km long profile across the shear zone is ~ 37 km (Fig. 5g), whereby ~ 14 km relative displacement occur across the central 50 m of the profile (Fig. 5h). D_r (Fig. 5g) and D_h (Fig. 5e) provide similar values for the shear zone which indicates that the deformation of the shear zones is close to simple shear and that the shear zone is responsible for most of the horizontal deformation.

To quantify the sensitivity of the results to different sediment viscosities and half-graben depths we performed additional numerical simulations. The results indicate that the sediment viscosity has a strong control on the kinematics of strain localization. If the top and bottom sediment layer have the same viscosity strain localization is significantly less intense (Figs. 6a–c, 7a–c). The strongest strain localization in the weak lower sediment layer was observed for viscosities of 10^{20} and 10^{21} Pa s and when the viscosity of the upper sediment layer was ten times larger (Figs. 4d, e, 6d, e). For a viscosity ratio between lower and upper sediment layer of 100 (10^{20} and 10^{22} Pa s, respectively, Fig. 7f) the maximum shear strain was smaller than for a viscosity ratio of 10 (10^{20} and 10^{22} Pa.s, respectively, Fig. 7d) which indicates that for the applied model configuration a viscosity ratio in the order of 10 provides the largest maximum shear strain and most intense strain localization. A reduction of the maximum half-graben depth from 5 to 1 km (not changing viscosities) had a minor impact on the values of the maximal shear strain and the strain localization which indicates a weak control of half-graben depth on strain localization (Fig. 8).

4 Discussion

The average amount of shear strain in basal shear zones of nappes can be estimated using the ratio of displacement over shear zone thickness. For example, Ebert et al. (2007) estimated a maximum displacement-thickness ratio of ~ 10 km/20 m = 500 for the Morcles nappe. The basal shear zone of the Glarus nappe recorded an average shear strain of about 30,000 (~ 30 km/1 m, e.g. Badertscher and Burkhard, 2000). In the presented models, the basal shear zone recorded maximum shear strains of at least 50 (one-layer sediments) and up to 750 (two-layer sediments; Fig. 5g, h), with an average of 280 (14 km/50 m) in the central shear zone (Figs. 4, 6). These values are of the same order of magnitude compared to values estimated for the Morcles nappe basal shear zone and ~ 40 times lower than the values for the Glarus thrust.

Values of shear strain of ~ 750 were obtained in the model with two layers of sediment (Fig. 7). The motivation for involving two sedimentary layers is to mimic the rheological layering in the sediments due to the brittle-ductile transition, that is, a more competent layer (around the brittle-ductile transition) resting above a less competent, ductile layer. Simulations with a more realistic viscoelastoplastic rheology inducing a dynamic brittle-ductile transition have been presented by Bauville and Schmalholz (2015; see Fig. 2), and their simulations provide similar results. The models with only one sedimentary layer recorded less intense strain in the shear zone than the two-layer models (Fig. 7). However, the value of shear strain in the one-layer model of up to ~ 60 for a shear zone a few hundred meter thick is still significant. Regarding the Glarus nappe basal shear zone, Ebert et al. (2007)

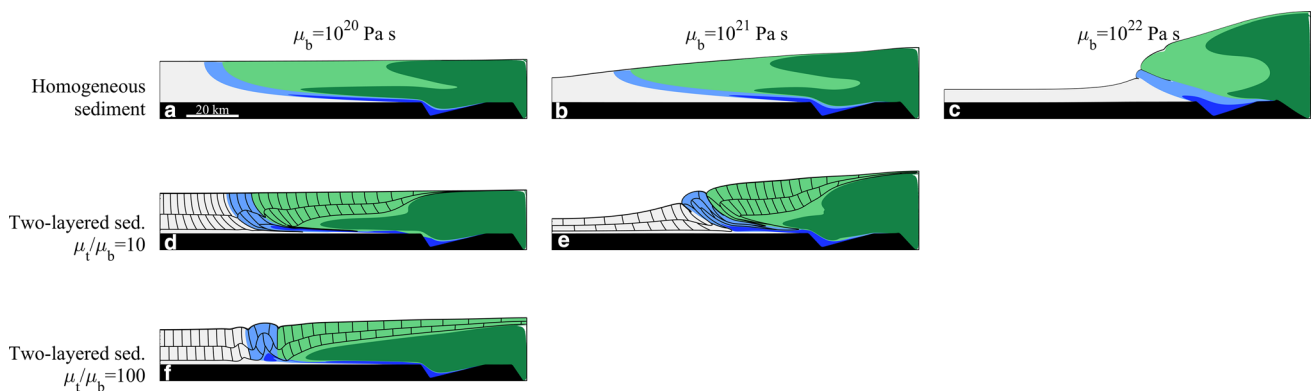


Fig. 6 Model results after 50% shortening for simulations with different sediment viscosities (model configuration is identical to the one shown in Fig. 3). The μ_t and μ_b are the viscosities of the top and bottom sediment layer, respectively. The top sediment layer is displayed with a limestone pattern when it has a viscosity different from that of the bottom layer. A–C: The μ_t and μ_b are identical and are 10^{20} Pa s (a), 10^{21} Pa s (b) and 10^{22} Pa s. d, e The μ_t is ten times

larger than μ_b (value is indicated at the top of the panel-column). F: The μ_t is hundred times larger than μ_b (value is indicated at the top of the panel-column). Lower sediment viscosities favor internal shearing while the model surface remains relatively flat (i.e. model domain remains more or less rectangular). Higher sediment viscosities favor wedge formation (i.e. considerable topography variation) while the internal shearing is less than for smaller viscosities

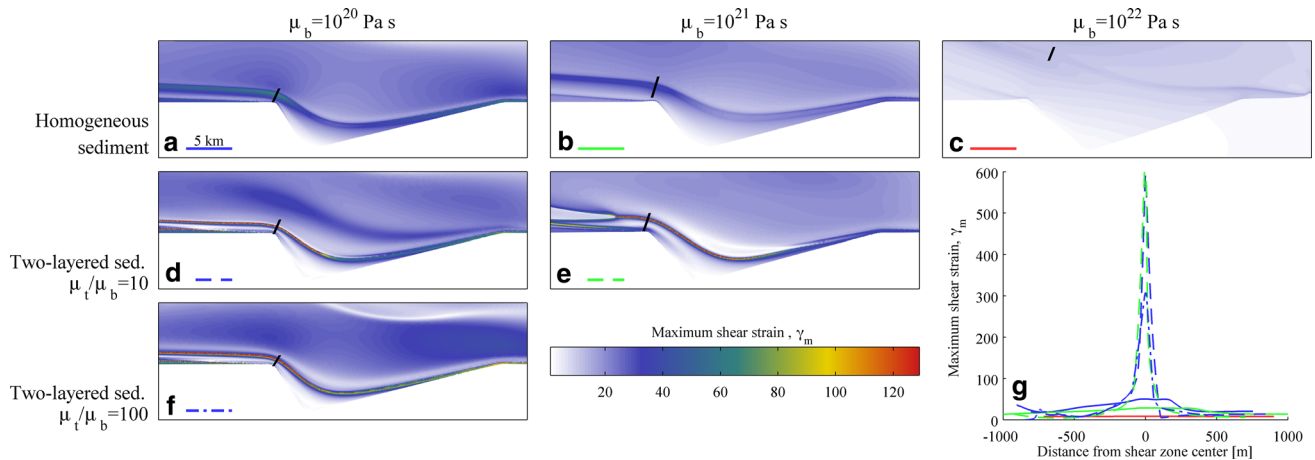


Fig. 7 Color plot of maximum shear strain (γ_m , Eq. 2) for simulations presented in Fig. 5. The enlargements show the same model region as in Fig. 4a–d. Kinematic strain localization occurs in all simulations. Strain localization is more intense for lower viscosities for homogeneous sediment viscosity (a–c). Strain localization is significantly larger for two sediment layers with different viscosities

(d–f). **g** Profile of maximum shear strain across the shear zone indicated as *black line* in figure a–f. The *line style* of the corresponding simulation is indicated in the *lower left corner* of panels a–f. The most intense strain localization with a maximum shear strain >500 is observed for the simulations with a viscosity ratio of 10 (d, e)

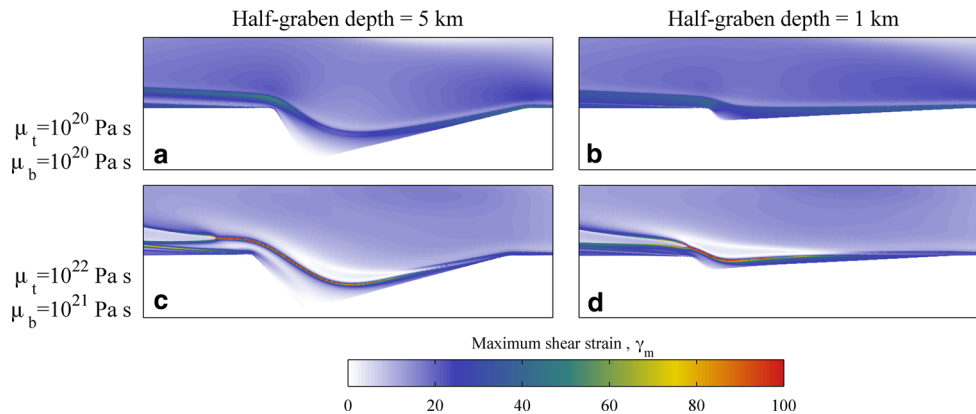


Fig. 8 Color plot of maximum shear strain after 50% shortening for simulations with different sediment viscosities (indicated at the left of each panel-row) and different half-graben depth (indicated at the top of each panel-column). The general model configuration is identical to the one shown in Fig. 3 (except half-graben depths and sediment viscosities). The enlargements show the same model region as in Fig. 4a–d. For different half-graben depths but identical viscosities

the maximum shear strain in the shear zone is similar (a, b and c, d) indicating a weak control of half-graben depth on kinematic strain localization. For different viscosities but identical half-graben depth the maximum shear strain in the shear zone is different (a, c and b, d) indicating a strong control of sediment viscosity on kinematic strain localization, which is in agreement with results shown in Fig. 6

concluded that microfabric modifications and exhumation induced cooling promoted further strain localization of an existing high-strain shear zone. Cooling would decrease the thickness of ductile sediments between the brittle-ductile transition in the sediments and the top of the basement. Our results suggest that the decrease of the distance between the depth of the brittle-ductile transition and the depth of the shear zone (i.e. a thinner weak sedimentary layer) would further localize strain. This additional strain localization effect, by thinning the ductile sedimentary layer, may have contributed to the intensification of shear localization described by Ebert et al. (2007).

The higher shear strain value in the basal shear zone obtained for the two-layer sediment model compared to the one-layer model may have two reasons:

1. The integral of strain over the area is the same for both models (background strain \times area). Therefore, if the upper, more competent layer deforms less, the lower layer has to deform more to obtain the same integrated strain of the entire model.
2. In the one-layer model any vertical profile of the horizontal velocity is similar to velocity profiles of channel flow models with a free surface (zero slip at the bottom, free surface at the top; e.g. Turcotte and

Schubert 2014). In the two-layer model, the velocity profile of the weak layer can be idealized as being bounded by a no slip condition at the bottom and a fixed horizontal velocity at the top which is imposed by the displacement of the upper layer. In this case, strain rate increases when the lower-layer thickness decreases (assuming that the top velocity is constant). Assuming a fixed depth of the upper layer, the thickness of the lower layer is smaller above horsts than it is above grabens. Therefore the weak layer records additional strain in the region above horsts.

The shear zones in the linear viscous sediments occur not only at the basement-cover interface but also entirely inside the linear viscous sediments where the shear zone extends across the sediments in the half-grabens (Fig. 5d). This shear zone formation inside linear viscous fluids is similar to the flow separation of a boundary layer, following the nomenclature of boundary layer theory (e.g. Batchelor 2000; Schlichting and Gersten 2017). Flow separation of the boundary layer shear zone from the boundary can occur if the boundary has sharp corners. Such sharp corners in the basement-cover interface are present in the models due to the half-graben geometry. In our model the separation of the shear zone is more intense around the steep slope of the half-graben geometry than around the shallow slope. The sharp corners along the basement-cover boundary are most likely responsible for the separation of the shear zone from the boundary and hence cause the shear zones within the linear viscous fluid which is sheared above this boundary. We argue that such flow separation could have played an important role during the shearing of less competent, ductile sediments over half-grabens and horsts whose geometry was defined by a more competent basement. Hence, such flow separation may have played an important role during nappe formation in the Helvetic nappe system.

A boundary layer forms in between a surface of no slip and a surface of zero stress condition at an infinite distance from the contact. Boundary layer thickness is generally defined as the limit at which the zero stress condition is satisfied at 99% and beyond which the flow can therefore be considered inviscid. In flow with Reynolds number >1 (typical for water or air) this thickness is in the order of mm to m. For the deformation of rocks at a geological time scale, however, the boundary layer thickness would be orders of magnitude larger than the earth (e.g. Batchelor 2000; Schlichting and Gersten 2017). Our model predicts a much thinner shear zone. The main difference with the boundary layer theory is that in our model the zero stress condition is satisfied at the free surface. A vertical velocity profile in the model is thus close to a channel flow with free surface (e.g. Turcotte

and Schubert 2014). Variations of the basement topography modify the depth at which the no slip condition is applied. This changes the vertical velocity profile and creates lateral variations in velocity, which, in turn, trigger kinematic strain localization.

Bauville and Schmalholz (2015) also performed viscous and more advanced viscoelastoplastic thermo-mechanical simulations in which the basement was more or less deformed. Their results suggest that a deformable basement does not significantly modify the kinematic strain localization due to basement topography, in particular during the initial stages of deformation.

Inversion of basins can occur by reactivation of normal faults as thrusts (Williams et al. 1989). Here, we did not consider a reactivation of normal faults since recent studies tend to agree that no significant reactivation of normal faults occurred in the external crystalline massifs (e.g. de De Graciansky et al. 1989; Butler 1989; Bauville and Schmalholz 2015).

Brittle thrusts, that is, faults controlled by a frictional, and not ductile, deformation are generally expected to dip upward. However, the basal shear zone of the Morcles nappe in places follows the irregular geometry of the Aiguilles-Rouges basement and is seen going down in today's orientation (although the original orientation of thrusting might have been different; e.g. Butler, 1992). Recent observations from the accretionary prism of the Japan Trench show that thrusts in shallow conditions can follow the topography and even step down into grabens (Boston et al. 2014). Whether the particular thrust imaged by Boston et al. (2014) follows a weaker sedimentary level or simply the basement topography, is unclear. Our results indicate that thrust-type shear zones can follow the basement topography and can also dip downwards (Fig. 5d).

Basement-cover half-graben geometry and ductile deformation outside the basal decollement are frequently neglected in accretionary wedge models based on brittle-plastic deformation (e.g. Buiter 2012; Graveleau et al. 2012). In such brittle-plastic wedge models the location and spacing of thrusts is entirely controlled by the geometry of the wedge and the associated internal stress distribution. However, when basement topography and/or basement deformation is taken into account it is systematically shown that basement topography has a strong control on the cover deformation, regardless of the considered rheology (e.g. Dominguez et al. 2000; Wissing and Pfiffner 2003; Panien et al. 2006; Bauville and Schmalholz 2015). In our model, the shear zones enabling the nappe emplacement are triggered by the basement topography and hence by the tectonic inheritance of former rifting phases. The geological reconstructions assigning individual nappes to different paleogeographic domains characterized by horst and half-graben structures supports the potential

importance of kinematic strain localization as an important trigger mechanism for the formation of tectonic nappes in the Helvetic nappe system.

5 Conclusion

We numerically studied the shearing of linear viscous fluids above a linear viscous fluid with considerably higher viscosity (quasi-undeformable) in two-dimensions. The boundary between the fluid (mimicking sediments) and the quasi-undeformable fluid (mimicking basement) exhibited geometrical perturbations (mimicking half-grabens). These geometrical perturbations can trigger significant strain localization and the formation of shear zones within the linear viscous fluid. This kinematic strain localization does not only occur at the interface between fluid and quasi-undeformable fluid but also entirely within the linear viscous fluid. If the fluid in contact with the quasi-undeformable fluid is overlain by a more viscous fluid, then the shear localization is more intense. The viscosity ratio between the fluid layers has a strong control on the kinematic strain localization, whereas the depth of the half-grabens has a weak control. The shear zones inside the fluid in contact with the quasi-undeformable fluid can exhibit a significant shear strain of up to 750 (i.e. ratio of shear displacement divided by shear zone thickness). For viscosities of the sheared fluid in the order of 10^{21} Pas and typical half-graben geometries of 5 km depth and 25 km width the kinematic strain localization generated a low-angle shear zone with a thickness in the order of 100 m and an associated lateral displacement of >10 km.

We applied the model to the pre-Alpine European passive margin and the formation of tectonic nappes in the Helvetic nappe system. The viscosity ratio in the model represents the competence ratio between basement and sediments and the geometrical perturbations mimic half-grabens. These half-grabens represent the tectonic inheritance of a former rifting event. The shear zones in the model generate structures comparable to sedimentary nappes which are sheared over the more proximal basement and sediments. The continuous shearing generates a stacking of the model nappes whereby the most distal nappes are structurally highest. The deformation sequence and nappe stacking in the simulations is in agreement with general observations from the Helvetic nappe system.

Tectonic inheritance in the form of half-grabens, competence contrast between basement and sediments, and ductile creep of the sediments can trigger and form ductile shear zones in the sediments during compression of the basement-sediment system even if there are no rheological

softening mechanisms active. The shear zones on which the nappes in the Helvetic nappe system have been displaced could have hence been triggered and controlled by the half-graben architecture of the pre-Alpine European passive margin. Such control by tectonic inheritance would agree with the common interpretation that the sediments composing individual nappes originated from different paleogeographical domains which were defined by the paleotopography of the basement. Tectonic inheritance and associated kinematic strain localization could therefore have been the trigger mechanism for nappe formation, and not a rheological softening mechanism. In contrast, softening mechanisms due to, for example, grain size reduction or shear heating, might have been activated during the early stages of kinematic strain localization and might have subsequently most likely further intensified the shear localization significantly.

Acknowledgements The authors thank Henri Masson, Yury Podladchikov, Neil Mancktelow and Marco Herwegh for helpful discussions; and Robert Butler, Christopher Beaumont and Stefan Schmid for constructive comments. This work was supported by Swiss National Fonds (SNF) grant no. 200021_131897, the University of Lausanne, the European Research Council under the European Community's Seventh Framework program (FP7/2007/2013) with ERC starting Grant Agreement No. 258830 and the SNF early Post-Doc. Mobility Grant No. 161927.

References

- Austin, N., Evans, B., Herwegh, M., & Ebert, A. (2008). Strain localization in the Morcles nappe (Helvetic Alps, Switzerland). *Swiss Journal of Geosciences*, 101(2), 341–360.
- Badertscher, N. P., & Burkhard, M. (2000). Brittle–ductile deformation in the Glarus thrust Lochseiten (LK) calc-mylonite. *Terra Nova*, 12(6), 281–288.
- Batchelor, G. K. (2000). *An introduction to fluid dynamics* (615 pp). Cambridge University Press.
- Bauville, A., Epard, J.-L., & Schmalholz, S.M. (2013). A simple thermo-mechanical shear model applied to the Morcles fold nappe (Western Alps). *Tectonophysics*, 583, 76–87.
- Bauville, A., & Schmalholz, S. M. (2015). Transition from thin-to thick-skinned tectonics and consequences for nappe formation: numerical simulations and applications to the Helvetic nappe system, Switzerland. *Tectonophysics*, 665, 101–117.
- Beer, F. P., & Erji, J. T. D. (2014). *Mechanics of Materials*. 7th edition.
- Bellanger, M., Bellahsen, N., Jolivet, L., Baudin, T., Augier, R., & Boutoux, A. (2014). Basement shear zones development and shortening kinematics in the Ecrins Massif. *Western Alps. Tectonics*, 33(2), 84–111.
- Boston, B., Moore, G. F., Nakamura, Y., & Kodaira, S. (2014). Out-rise normal fault development and influence on near-trench décollement propagation along the Japan Trench, off Tohoku. *Earth, Planets and Space*, 66(135), 1–17.
- Boutoux, A., Bellahsen, N., Lacombe, O., Verlaquet, A., & Mouthereau, F. (2014). Inversion of pre-orogenic extensional basins in the external Western Alps: Structure, microstructures and restoration. *Journal of Structural Geology*, 60, 13–29.

- Bower, A. F. (2009). *Applied mechanics of solids*. CRC press.
- Braun, J., Herman, F., & Batt, G. (2010). Kinematic strain localization. *Earth and Planetary Science Letters*, 300(3), 197–204.
- Brun, J. P. (2002). Deformation of the continental lithosphere: Insights from brittle-ductile models. *Geological Society, London, Special Publications*, 200(1), 355–370.
- Brun, J. P., & Merle, O. (1985). Strain patterns in models of spreading-gliding Nappes. *Tectonics*, 4(7), 705–719.
- Bucher, W. H. (1956). Role of gravity in orogenesis. *Geological Society of America Bulletin*, 67(10), 1295–1318.
- Bugnon, P.-C. (1986). *Géologie de l'helvétique à l'extrémité sud-ouest du massif de l'Aar (Loèche, Valais)* [PhD thesis], Lausanne, Université de Lausanne, 106 p.
- Buiter, S. J. (2012). A review of brittle compressional wedge models. *Tectonophysics*, 530, 1–17.
- Butler, R. W. H. (1989). The influence of pre-existing basin structure on thrust system evolution in the Western Alps. *Geological Society, London, Special Publications*, 44(1), 105–122.
- Butler, R. W. (1992). Evolution of Alpine fold-thrust complexes: a linked kinematic approach. In: S. Mitra & G. W. Fisher (Eds.), *Structural geology of fold and thrust belts* (pp. 29–44). Hopkins University Press.
- Dabrowski, M., Krotkiewski, M., & Schmid, D. W. (2008). MILAMIN: MATLAB-based finite element method solver for large problems. *Geochemistry, Geophysics, Geosystems*, 9(4), 1–24.
- De Graciansky, P. C., Dardeau, G., Lemoine, M., & Tricart, P. (1989). The inverted margin of the French Alps and foreland basin inversion. *Geological Society, London, Special Publications*, 44(1), 87–104.
- Dominguez, S., Malavieille, J., & Lallemand, S. E. (2000). Deformation of accretionary wedges in response to seamount subduction: Insights from sandbox experiments. *Tectonics*, 19(1), 182–196.
- Dumont, T., Champagnac, J.-D., Crouzet, C., & Rochat, P. (2008). Multistage shortening in the Dauphiné zone (French Alps): the record of Alpine collision and implications for pre-Alpine restoration. *Swiss Journal of Geosciences*, 101, S89–S110.
- Duretz, T., Kaus, B. J. P., Schulmann, K., Gapais, D., & Kermarrec, J. J. (2011). Indentation as an extrusion mechanism of lower crustal rocks: Insight from analogue and numerical modelling, application to the Eastern Bohemian Massif. *Lithos*, 124(1), 158–168.
- Ebert, A., Herwegh, M., Berger, A., & Pfiffner, A. (2008). Grain coarsening maps for polyminerale carbonate mylonites: a calibration based on data from different Helvetic nappes (Switzerland). *Tectonophysics*, 457(4), 128–142. doi:10.1016/j.tecto.2008.05.007.
- Ebert, A., Herwegh, M., & Pfiffner, A. (2007). Cooling induced strain localization in carbonate mylonites within a large-scale shear zone (Glarus thrust, Switzerland). *Journal of Structural Geology*, 29(7), 1164–1184.
- Epard, J.-L., 1990. *La Nappe de Morcles au Sud-Ouest du Mont-Blanc* (165 pp.). Mémoires de Géologie (Lausanne) 8.
- Escher, A., Masson, H., & Steck, A. (1993). Nappe geometry in the western Swiss Alps. *Journal of Structural Geology*, 15(3), 501–509.
- Frehner, M., & Schmalholz, S. M. (2006). Numerical simulations of parasitic folding in multilayers. *Journal of Structural Geology*, 28(9), 1647–1657.
- Gillierist, R., Coward, M., & Mugnier, J. L. (1987). Structural inversion and its controls: examples from the Alpine foreland and the French Alps. *Geodinamica Acta*, 1(1), 5–34.
- Graveleau, F., Malavieille, J., & Dominguez, S. (2012). Experimental modelling of orogenic wedges: A review. *Tectonophysics*, 538, 1–66.
- Herwegh, M., Hürzeler, J. P., Pfiffner, O. A., Schmid, S. M., Abart, R., & Ebert, A. (2008). the Glarus thrust: excursion guide and report of a field trip of the Swiss tectonic studies Group (Swiss Geological society, 14–16. 09. 2006). *Swiss Journal of Geosciences*, 101(2), 323–340.
- Herwegh, M., & Pfiffner, O. A. (2005). Tectono-metamorphic evolution of a nappe stack: A case study of the Swiss Alps. *Tectonophysics*, 404, 55–76.
- Huqi, L., McClay, K. R., & Powell, D. (1992). Physical models of thrust wedges. In K. R. McClay (Ed.), *Thrust tectonics* (pp. 71–81). Netherlands: Springer.
- Kirschner, D. L., Sharp, Z. D., & Masson, H. (1995). Oxygen isotope thermometry of quartz-calcite veins: Unraveling the thermal-tectonic history of the subgreenschist facies Morcles nappe (Swiss Alps). *Geological Society of America Bulletin*, 107(10), 1145–1156.
- Mase, G. E. (1970). *Schaum's outline of theory and problems of continuum mechanics*. New York: McGraw-Hill.
- Masson, H., Herb, R., & Steck, A. (1980). Helvetic Alps of Western Switzerland. In R. Trümpy (Ed.), *Geology of Switzerland, A Guide Book (Part B)* (pp. 109–153). Basel: Wepf.
- Ménot, R. P., Von Raumer, J. F., Bogdanoff, S., & Vivier, G. (1994). Variscan basement of the Western Alps: the external Crystalline Massifs. In J. D. Keppie (Ed.), *Pre-Mesozoic Geology in France and Related Areas* (pp. 458–466). Berlin Heidelberg: Springer.
- Merle, O. (1986). Patterns of stretch trajectories and strain rates within spreading-gliding nappes. *Tectonophysics*, 124(3), 211–222.
- Merle, O., & Guillier, B. (1989). The building of the Central Swiss Alps: an experimental approach. *Tectonophysics*, 165(1), 41–56.
- Panien, M., Buiter, S. J. H., Schreurs, G., & Pfiffner, O. A. (2006). Inversion of a symmetric basin: insights from a comparison between analogue and numerical experiments. *Geological Society, London, Special Publications*, 253(1), 253–270.
- Pfiffner, O. A. (1993). The structure of the Helvetic nappes and its relation to the mechanical stratigraphy. *Journal of Structural Geology*, 15(3), 511–521.
- Pfiffner, O. A., Burkhard, M., Hänni, R., Kammer, A., Kligfield, R., Mancktelow, N. S., Menkveld, J. W., Ramsay, J. G., Schmid, S. M., & Zurbiggen, R. (2011). *Structural map of the Helvetic Zone of the Swiss Alps, including Vorarlberg (Austria) and Haute Savoie (France), 1: 100'000*. Geological Special Map 128. Bundesamt für Landestopografie swisstopo.
- Poirier, J. P. (1980). Shear localization and shear instability in materials in the ductile field. *Journal of Structural Geology*, 2(1), 135–142.
- Poulet, T., Veveakis, M., Herwegh, M., Buckingham, T., & Regenauer-Lieb, K. (2014). Modeling episodic fluid-release events in the ductile carbonates of the Glarus thrust. *Geophysical Research Letters*, 41(20), 7121–7128.
- Prandtl, L. (1904). Über Flüssigkeitsbewegung bei sehr kleiner Reibung. *Verhandlungen des III. Internationalen Mathematiker-Kongresses, Heidelberg*, (B. G. Teubner, Leipzig), 484–491.
- Ragan, D. M. (2009). *Structural Geology, an introduction to geometrical techniques* (p. 602). Cambridge University Press, Cambridge.
- Schlichting, H., & Gersten, K. (2017). *Boundary-layer theory*. 9th edition. Springer Science & Business Media.
- Schmalholz, S. M., Duretz, T., Schenker, F. L., & Podladchikov, Y. Y. (2014). Kinematics and dynamics of tectonic nappes: 2-D numerical modelling and implications for high and ultra-high pressure tectonism in the Western Alps. *Tectonophysics*, 631, 160–175.
- Shewchuk, J. R. (2002). Delaunay refinement algorithms for triangular mesh generation. *Computational geometry*, 22(1), 21–74.

- Siegenthaler, C. (1974). *Die Nordhelvetische Flysch-Gruppe im Sernftal (Kt. Glarus)*. Ph.D. Thesis, University of Zürich, 83 pp.
- Steck, A. (1984). Structures et déformations tertiaires dans les Alpes Centrales (transversale Aar-Simplon-Ossola). *Eclogae Geologicae Helvetiae*, 77, 55–100.
- Townend, J., & Zoback, M. D. (2000). How faulting keeps the crust strong. *Geology*, 28(5), 399–402.
- Trümpy, R. (1960). Paleotectonic evolution of the Central and Western Alps. *Geological Society of America Bulletin*, 71(6), 843–907.
- Turcotte, D. L., & Schubert, G. (2014). *Geodynamics*. Cambridge University Press.
- Williams, G. D., Powell, C. M., & Cooper, M. A. (1989). Geometry and kinematics of inversion tectonics. *Geological Society, London, Special Publications*, 44, 3–15.
- Wissing, S. B., & Pfiffner, O. A. (2003). Numerical models for the control of inherited basin geometries on structures and emplacement of the Klippen nappe (Swiss Prealps). *Journal of Structural Geology*, 25(8), 1213–1227.